ARTICLE

Photodissociation Dynamics of Nitrous Oxide: The $O(^1D) + N_2(X^1\Sigma_g^+)$ Product Channel†

Shuaikang Yang[a,b], Yucheng Wu[b], Zijie Luo[b,c], Zhenxing Li[b], Wei Hua[b], Yao Chang[b], Xingan Wang[a*], Kaijun Yuan[b,d*], Xueming Yang[b,d,e]

a. Department of Chemical Physics, School of Chemistry and Materials Science, University of Science and Technology of China, Hefei 230026, China
b. State Key Laboratory of Molecular Reaction Dynamics and Dalian Coherent Light Source, Dalian Institute of Chemical Physics, Chinese Academy of Sciences, Dalian 116023, China
c. Marine Engineering College, Dalian Maritime University, Dalian 116026, China
d. Hefei National Laboratory, Hefei 230088, China
e. Department of Chemistry and Center for Advanced Light Source Research, College of Science, Southern University of Science and Technology, Shenzhen 518055, China

(Dated: Received on December 22, 2023; Accepted on January 10, 2024)

Photodissociation of nitrous oxide (N_2O) in the ultraviolet region has been revisited by using the time-sliced velocity map ion imaging technique, due to its importance in atmospheric chemistry. The images of $O(^1D)$ photofragments are recorded at 203.814 nm and 205.472 nm in one-color experiments and at eight photolysis wavelengths between 200 and 220 nm in two-color experiments. The rotational state distributions and angular anisotropy parameters of the $N_2(X^1\Sigma_g^+)$ co-products are derived from the images. The results indicate that the rotational state distributions are inverted with the maximum around $J\approx70$. The anisotropy parameter β mainly shows two declines as the N_2 rotational quantum number J increases. According to theoretical calculations [J. Chem. Phys. **136**, 044314 (2012)], the variations in β with J are caused by changes in the extent of axial recoil from a linear initial configuration. In the high-J region, however, additional torque exists on the ground state potential energy surface following nonadiabatic transitions, inducing both the additional rotational excitation and the lower β values. Compared to previous works, the two-color experiments combined with single vacuum ultraviolet photonionization of $O(^1D)$ allow us to acquire both the rotational state distribution and angular distribution accurately. This work deepens our understanding of triatomic molecule decomposition.

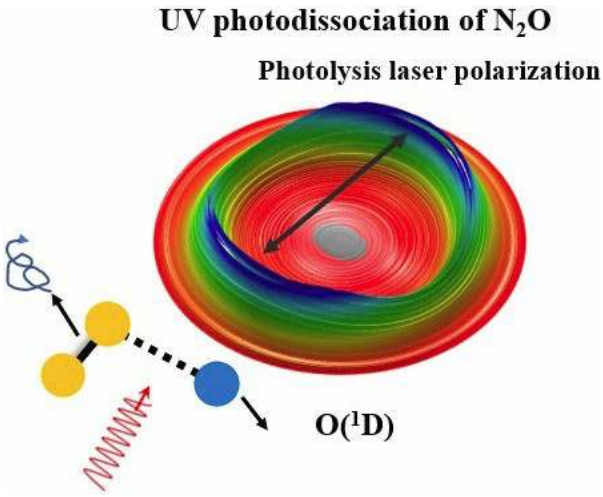

Key words: Ultraviolet photodissociation, Nitrous oxide, Time-sliced velocity map ion imaging

I. INTRODUCTION

Nitrous oxide (N_2O) is the third most powerful greenhouse gas after carbon dioxide (CO_2) and methane

† Part of Special Issue "In Memory of Prof. Qihe Zhu on the occasion of his 100th Aniversary".

* Authors to whom correspondence should be addressed. E-mail: kjyuan@dicp.ac.cn, xawang@ustc.edu.cn

(CH_4), which plays a vital role in the Earth's atmosphere. Due to its long lifetime (~118±7 years), its global warming potential is nearly 300 times that of carbon dioxide [1–3]. Natural emissions of N_2O mainly originate from bacterial nitrification and denitrification reactions in soil and oceans [4]. Its anthropogenic sources include agricultural production, biofuel burning, and industrial activities such as chemical production. Many relevant studies indicate that anthropogenic sources of N_2O account for approximately 43% of global emissions, and the croplands provide more than 40% of anthropogenic emissions into the atmosphere, whose contribution is larger than any other anthropogenic sources [5, 6]. Photolysis from 195 nm to 215 nm in the stratosphere makes up about 90% of atmospheric sink for N_2O (*i.e.*, the removal process), while the remaining is eliminated by reacting with $O(^1D)$ [7, 8]. Recent investigations [9, 10] speculated that the oxygen production from N_2O photolysis may provide the initial O_2 that induces the "Great Oxidation Event", which is an additional abiotic oxygen production mechanism, besides the photolysis of CO_2, H_2O, and SO_2 [11–15].

Photodissociation of N_2O in the first absorption band between 222 nm and 170 nm has been extensively investigated both experimentally and theoretically in the past decades. This absorption band has a broad Gaussian shape superimposed with some weak diffuse vibrational structures [16], which has been attributed to the transition from the ground state $^1\Sigma^+$ ($1^1A'$ in bent geometry) to the $^1\Sigma^-$ state ($1^1A''$, $T_e = 6.81$ eV) and the $^1\Delta$ state ($T_e = 6.97$ eV). The doubly degenerate linear $^1\Delta$ state is split into $2^1A'$ and $2^1A''$ components in bent geometry due to the Renner-Teller effect [17]. According to the theoretical calculations [18–20], the transitions from the ground state to $^1\Sigma^-$ and $^1\Delta$ are dipole forbidden in linear configurations with $C_{\infty v}$ symmetry and weakly allowed in bent configurations with C_s symmetry [20]. Therefore, the absorption spectrum in the ultraviolet region primarily involves the excitation of $1^1A'$ to $1^1A''$ and $2^1A'$ states. While the $2^1A''$ state has a linear equilibrium configuration and increases in energy upon bending, it is not dissociative near 200 nm [21–23].

Photodissociation of N_2O around 200 nm forms almost exclusively oxygen atoms in the excited ^1D state and N_2 molecules in the ground electronic state [17],

$$N_2O + h\nu(\sim 200\ \text{nm}) \rightarrow O\left(^1D\right) + N_2\left(X^1\Sigma_g^+\right) \quad (1)$$
$$D_0 = 3.699\ \text{eV}$$

The energetically more favorable but spin-forbidden channel of $N_2(X^1\Sigma_g^+)$ and ground state oxygen $O(^3P)$, has a negligible quantum yield in this wavelength region. Previous studies showed that the branching ratio of the $O(^3P)$ channel is less than 2.5% at photolysis wavelengths between 184.9 nm and 213.9 nm [24–26]. More detailed dynamics experiments have been carried out in several wavelengths (193 nm, 203 nm, and 205 nm), to measure the energetics and spatial distributions of the $O(^1D)$ fragments [27–32]. By using the time-of-flight mass spectrometry, Felder *et al.* [27] indicated that the $O(^1D)$ velocity distribution produced in the 193 nm photolysis could be characterized by a positive angular anisotropy parameter, $\beta = 0.48$, and ~42% of the available energy was found in the translational energy of the fragments. Springsteen *et al.* [28] also studied photodissociation of N_2O at 193 nm using Doppler spectroscopy of $O(^1D)$ fragments, yielded $\beta \approx 0.50$. Hanisco *et al.* [29] then detected N_2 fragments from N_2O photolysis around 202–204 nm by using resonance enhanced multiphoton ionization (REMPI), and found that the internal energy of N_2 deposits exclusively in the rotational degree of freedom.

In 1996, Suzuki *et al.* [30] reported one-color two-dimensional ion imaging at 205 nm photolysis of N_2O, in which two components with different β values were observed in the recoil velocity distribution of $O(^1D)$ fragments. In 1999, Neyer *et al.* [31] applied an improved velocity mapping technique to study the photodissociation of N_2O around 203–205 nm, and found the J-dependent angular anisotropy parameter for the N_2 fragments which decreases with increasing the rotational quantum number. In 2004, Nishide *et al.* [32] displayed partially resolved rotational distribution of N_2 fragments by using velocity map ion imaging of $O(^1D)$ and 2+1 REMPI of N_2. The maximum of the N_2 rotational distribution shifted from $J = 72$ to 74 in changing the photolysis wavelength from 205.5 nm to 203.8 nm. These results revealed complicated photodissociation dynamics involved in the formation of $O(^1D) + N_2(X^1\Sigma_g^+)$ fragments.

However, due to the REMPI detection of $O(^1D)$ being sensitive to electron orbital alignment, the images observed through different REMPI transitions via $^1P_1$ and $^1F_3$ exhibited markedly different patterns, while the REMPI detection of N_2 has different transition probability for different rotational states which prevents acquiring accurate rotational distributions of N_2.

DOI: 10.1063/1674-0068/cjcp2312135

In this work, photodissociation of N_2O has been revisited in one-color experiments at 203.814 nm and 205.472 nm using 2+1 REMPI of $O(^1D)$ fragments, and in two-color experiments with the photolysis wavelength between 200–220 nm using single vacuum ultraviolet (VUV) photonionization of $O(^1D)$ combined with time-sliced velocity map ion imaging method. From the ion images, the rotational state distributions of N_2 fragments and the rotational state dependent anisotropy parameters are determined. This study deepens our understanding of dissociation dynamics of such important photochemical processes in earth atmosphere.

II. EXPERIMENTS

The experiment apparatus used in this study has been described in previous publications [33–38]. In brief, the pulsed supersonic molecular beam was generated by expanding the gas mixture (5%N_2O in Ar) into the source chamber via a pulsed valve with a 0.5 mm orifice, where it was skimmed before entering and propagating along the center axis of the ion optics assembly (IOA, 23-plate ion optics) mounted in the reaction chamber. The molecular beam was orthogonal to the photolysis and probe laser beams, which were coplanar and intersected each other at a certain angle between the second and third plates of the ion optics assembly. The N_2O molecules were photodissociated by absorbing one photon of 200–220 nm. After a delay time of 15 ns, the $O(^1D)$ fragments were state-selectively ionized by an autoionization ($\lambda = 99.95$ nm) scheme. Then the O^+ ions were accelerated through an electric filed manufactured by the IOA and flied 760 mm along the center axis of the IOA before impacting a dual microchannel plate (MCP) coupled with a P47 phosphor screen. The instantaneous images on the phosphor screen were captured and recorded by a charge-coupled device (CCD) camera. The MCP was driven by a high pulsed voltage, and the gate was 15–20 ns.

In this work, the UV photolysis laser originated from a frequency tripled pulsed dye laser pumped by the second harmonic output of the Nd:YAG laser (532 nm). The VUV probe laser was generated from a sum frequency four-wave mixing (FWM) scheme, involving two 249.63 nm photons and one 501.72 nm photon that were overlapped in space and time using Xe as the nonlinear medium. The other Nd:YAG laser (355 nm) pumped two dye lasers to produce 501.72 nm and 499.26 nm lasers respectively. The laser at 249.63 nm was generated by frequency doubling the 499.26 nm laser, using a BBO crystal. The polarization directions of both the photolysis laser and the probe laser were parallel to the plane of the detector.

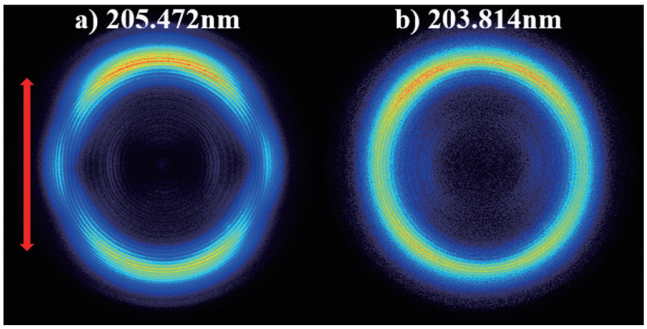

FIG. 1 The time-sliced velocity mapped ion images of $O(^1D)$ products from one-color laser photolysis of N_2O at 205.472 nm and 203.814 nm, respectively. The vertical arrow represents the polarization direction of the photolysis laser.

III. RESULTS AND DISCUSSION

We first reinvestigated photolysis of N_2O in one-color experiments at 203.814 nm and 205.472 nm. FIG. 1 shows the time-sliced ion images of $O(^1D)$ photofragments, which are detected by two-photon excitation to the $^1F_3$ and $^1P_1$ states at 203.814 nm and 205.472 nm, *i.e.*, the REMPI detection via the $^1F_3 \leftarrow {}^1D$ and $^1P_1 \leftarrow {}^1D$ respectively. The red double arrow in FIG. 1 is the polarization direction of the photolysis laser. Many fine concentric rings can be observed in the images, which correspond to the rotational states of co-products $N_2(X^1\Sigma_g^+)$. Compared with previous studies [32, 39–42], our $O(^1D)$ fragment images have higher resolution. A lot of structures in the weak inner rings of images, which are ascribed to high rotational states of $N_2(X^1\Sigma_g^+,\ v=0,\ J>80)$ fragments, can be clearly seen in the perpendicular direction. These highly rotationally excited N_2 fragments have only been observed by 2+1 REMPI of N_2 in previous works [29, 31, 32, 40, 43]. The maximum populated rotational quantum numbers of N_2 are $J_{max} = 99$ for $v = 0$, and $J_{max} = 90$ for $v = 1$. Previous studies by Kawamata *et al.* [40] also presented high-resolution $O(^1D)$ images by using the pBASEX method, but the population of highly rotationally excited N_2 seems to be underestimated.

FIG. 2 displays the total kinetic energy release (TKER) spectra derived from images shown in FIG. 1. To

DOI: 10.1063/1674-0068/cjcp2312135

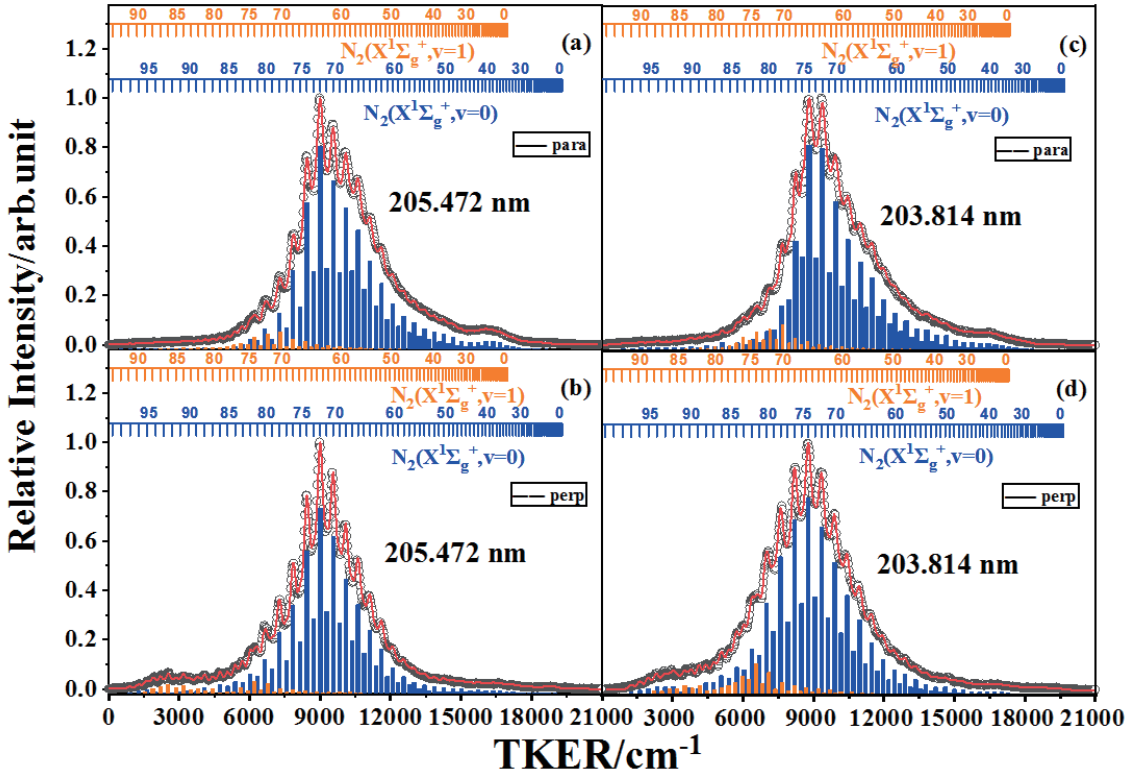

FIG. 2 The corresponding TKER spectra for the $O(^1D)+N_2(X^1\Sigma_g^+)$ channel from photodissociation of N_2O derived from those images shown in FIG. 1. (a, c) and (b, d) are extracted from images by integrating angles from −15° to 15° (parallel relative to the laser polarization) and from 75° to 105° (perpendicular), respectively. The experimental and fitting spectra are plotted as open circles and red solid lines, respectively. The superposed combs indicate the TKER values associated with formation of the various $N_2(X^1\Sigma_g^+, v=0, 1)$. The stick spectra in blue and orange shown underneath the experimental curves are rotational distributions of $N_2(X^1\Sigma_g^+, v=0, 1)$ products.

acquire higher resolution, FIG. 2 (a, c) and (b, d) are extracted from images by integrating signals between angles of −15° and 15°, and between 75° and 105° relative to the photolysis laser polarization, which are marked as "para" and "perp". The TKER spectra can then be converted to the internal energy spectra of the $N_2(X^1\Sigma_g^+)$ fragments through the following expression,

$$\begin{aligned} E_{h\nu} - D_0 &= E_T(O) + E_T(N_2) + E_{int}(N_2) \\ &= \text{TKER} + E_{int}(N_2) \end{aligned} \quad (2)$$

where D_0 is the dissociation energy for the $O(^1D)+N_2(X^1\Sigma_g^+)$ channel from N_2O photodissociation, $E_{int}(N_2)$ is the internal energy of $N_2(X^1\Sigma_g^+)$ fragments, and $E_T(O)$ and $E_T(N_2)$ are the kinetic energy of $O(^1D)$ and $N_2(X^1\Sigma_g^+)$ fragments respectively. The stick spectra underneath the experimental spectra represent the rotational state distributions of the $N_2(X^1\Sigma_g^+)$ products returned by fitting the TKER spectra. The rotational state population alternation of 2:1 is due to nuclear spin statistics of $^{14}N_2$. It is obvious that the N_2 products are dominantly populated in high rotational levels from $J\approx30$ to $J=99$, with peaking at $J=74$ (203.814 nm) and $J=72$ (205.472 nm) for $v=0$. While a small portion of N_2 distributes in $v=1$ with the rotational quantum number between $J\approx50$ and $J=90$, and the maximum population is near $J\approx70$. These are consistent with previous studies, in which Hanisco *et al.* [29] reported that the $N_2(X^1\Sigma_g^+)$ fragments in $v=0$ and $v=1$ states are produced, and predicted that the population of vibrationally excited N_2 is less than 2% of its vibrational ground state. It is known that the ground, $1^1A''$, and $2^1A'$ states all correlate adiabatically to $O(^1D)+N_2(X^1\Sigma_g^+)$ products, but the avoided crossings between $2^1A'/1^1A''$ states and $1^1A'$ state induce the initially excited N_2O transferring to $1^1A'$ state and then dissociating on this state. Due to the transitions from the ground state to the $2^1A'$ and $1^1A''$ states requiring a configuration change from linear to bent, a large torque exerts on molecule during dissociation, resulting in N_2 product with high rotational excitation [19, 23, 44]. Theoretical calculations by Schmidt *et al.* and Schinke

DOI: 10.1063/1674-0068/cjcp2312135

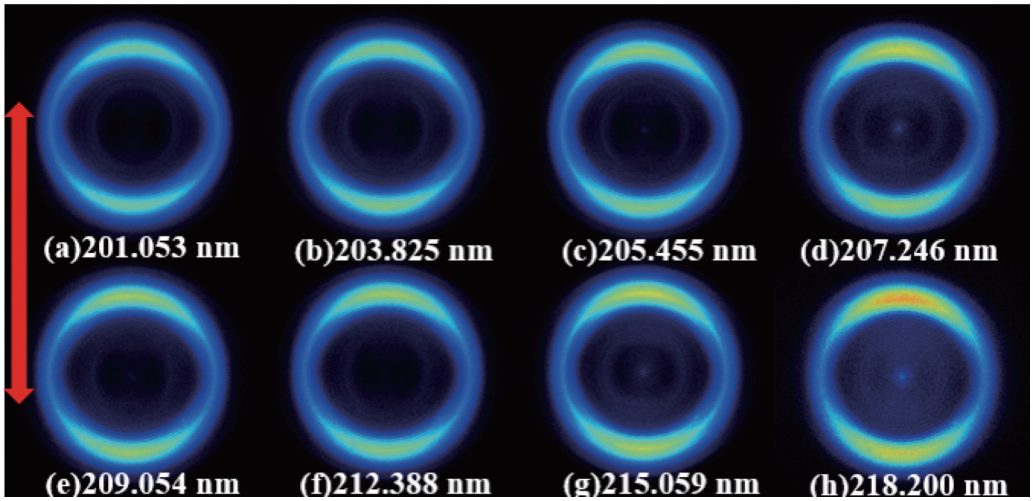

FIG. 3 The time-sliced velocity mapped ion images of $O(^1D)$ products from two-color laser photolysis of N_2O at (a) 201.053 nm, (b) 203.825 nm, (c) 205.455 nm, (d) 207.246 nm, (e) 209.054 nm, (f) 212.388 nm, (g) 215.059 nm and (h) 218.200 nm, respectively. The $O(^1D)$ products are resonantly ionized at λ=99.95 nm. The vertical arrow represents the polarization direction of the photolysis laser.

et al. [22, 44] confirmed that the N_2 fragments from N_2O photolysis at 204 nm via the $2^1A'$ state populate in two vibrational states with high rotational excitation, while those produced through the $1^1A''$ state have hotter vibrational excitation ($v\leq4$) and cooler rotational excitation. The N_2 products with vibrational excitation $v>1$ have not been observed experimentally, which suggests that the $1^1A''$ state may play a minor role in the N_2O dissociation in this wavelength region.

The difference between $O(^1D)$ images at 203.814 nm and 205.472 nm in one-color experiments is evident. According to previous work [39], it can be attributed to the different alignment of the atomic intermediate state before ionization, rather than the inherent property of dissociation dynamics at these two photolysis wavelengths. The ionization efficiency of $O(^1D)$ atoms in different spatial regions is different. In some regions, $O(^1D)$ atoms are easy to ionize, while in other regions $O(^1D)$ atoms are hard to ionize. The $O(^1D)$ images obtained by 2+1 REMPI scheme from N_2O photolysis at 203.814 nm and 205.472 nm are similar to that from photolysis of NO_2 and O_2 molecules [45, 46]. In order to uncover the "veils" cast on the spatial distributions of the products by the alignment effect and acquire the true spatial and state distributions from N_2O photolysis, we choose to ionize $O(^1D)$ atoms via the autoionization scheme at 99.95 nm atomic spectra line ($^1P_1\leftarrow{}^1D$) [47]. There is no change in the images with varying the polarization direction of the probe laser, confirming that this detection method itself has no additional impact on the experimental results. FIG. 3 shows $O(^1D)$ fragment images from photolysis of N_2O in two-color experiments between 200 nm and 220 nm. These images from eight photolysis wavelengths are quite similar with each other. The anisotropy of these images is larger than that at 203.814 nm in one-color experiments. In addition, the dimples observed in perpendicular direction at 205.472 nm in one-color experiments clearly disappear, which suggests the influence arising from the detection process caused by alignment of the product at 203.814 nm and 205.472 nm has been removed in two-color experiments.

The corresponding TKER spectra derived from the images in FIG. 3 are shown in FIG. 4. It is noted that only the TKER spectra in the direction with the best resolution are shown here, *i.e.*, perpendicular for 201–209 nm and parallel for 212–218 nm. No observable structures correspond to the rotational states of $N_2(v=1)$ fragments due to the limited resolution. Therefore, the fitting spectra do not involve the minor population of $N_2(v=1)$. As is common in photodissociation, the maximum for rotational state distributions shifts to higher J with increasing photon energy. The rotational distributions computed by Schmidt *et al.* [44] using only the $2^1A'$ state had an asymmetric bell shape, which ended abruptly at a maximum value of J near 80. In comparison, the rotational state distributions shown either in parallel or in perpendicular direction display only a little asymmetry, and a higher J tail ($J>90$) can be seen, suggesting the theoretical calculations underes-

DOI: 10.1063/1674-0068/cjcp2312135

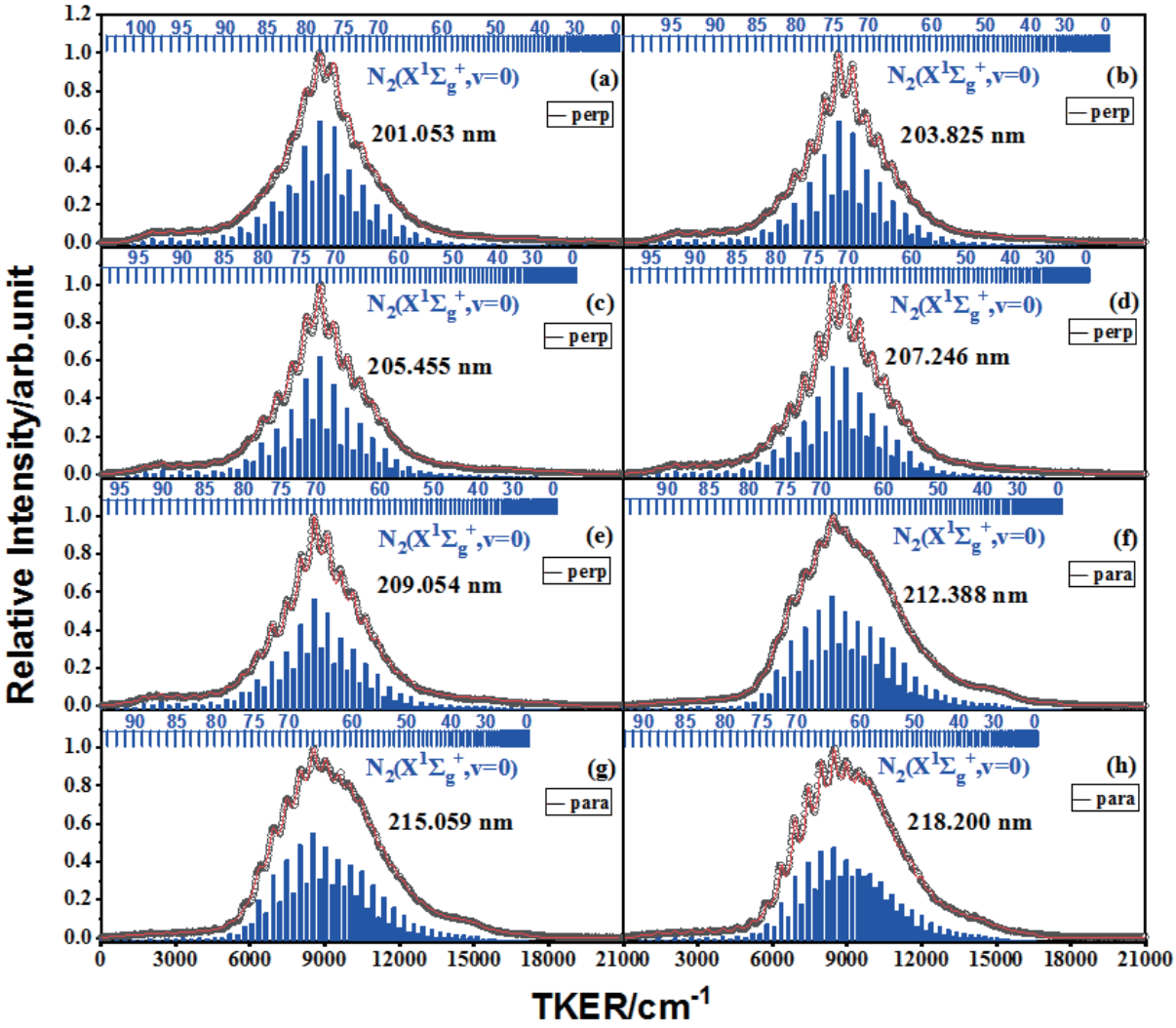

FIG. 4 The corresponding TKER spectra for the $O(^1D)+N_2(X^1\Sigma_g^+)$ channel from photodissociation of N_2O derived from those images shown in FIG. 3. The experimental and fitting spectra are plotted as open circles and red solid lines, respectively. The superposed combs indicate the TKER values associated with formation of the various $N_2(X^1\Sigma_g^+, v=0)$. The stick spectra in blue shown underneath the experimental curves are rotational distributions of $N_2(X^1\Sigma_g^+, v=0)$ products.

timate the high-J population.

The photodissociation anisotropy parameter β has also been acquired in the images, which provides information about the detailed reaction mechanism. McBane *et al.* [23] pointed out that absorption to the $1^1A''$ state would produce $\beta=-1$ due to the transition dipole being perpendicular to the triatomic plane; while absorption to the $2^1A'$ state, whose transition dipole lies in the triatomic plane, could produce any value of β, depending on the angle between the transition dipole moment and the molecular axis. Nishide *et al.* [32] interpreted their β observations on N_2O in terms of relative contributions of $2^1A'$ and $1^1A''$ states to the dissociation. They assumed $\beta=1.8$ for dissociation on $2^1A'$ state in analogy with that observed in OCS photodissociation, and concluded that absorption to $1^1A''$ state contributed about 30% based on β value at 205.472 nm. Kawamata *et al.* [40] further demonstrated that the β value of 1.8 corresponds to the angle between the recoil velocity of the product fragments and the dipole moment being about 15°. If a larger angle is employed, such as 30°, the corresponding β value is 1.25, then the estimated contribution of the $1^1A''$ state to dissociation is around 10%. This ratio is still much higher than the theoretical prediction of initial excitation to the two electronic states. Theoretical calculations [22, 48] predicted that the contribution of the $1^1A''$ state to dissociation is less than 3%. The discrepancy may come from the fixed β value used in estimating the contribution of these two states. Perhaps, it can be considered that the two states have

DOI: 10.1063/1674-0068/cjcp2312135

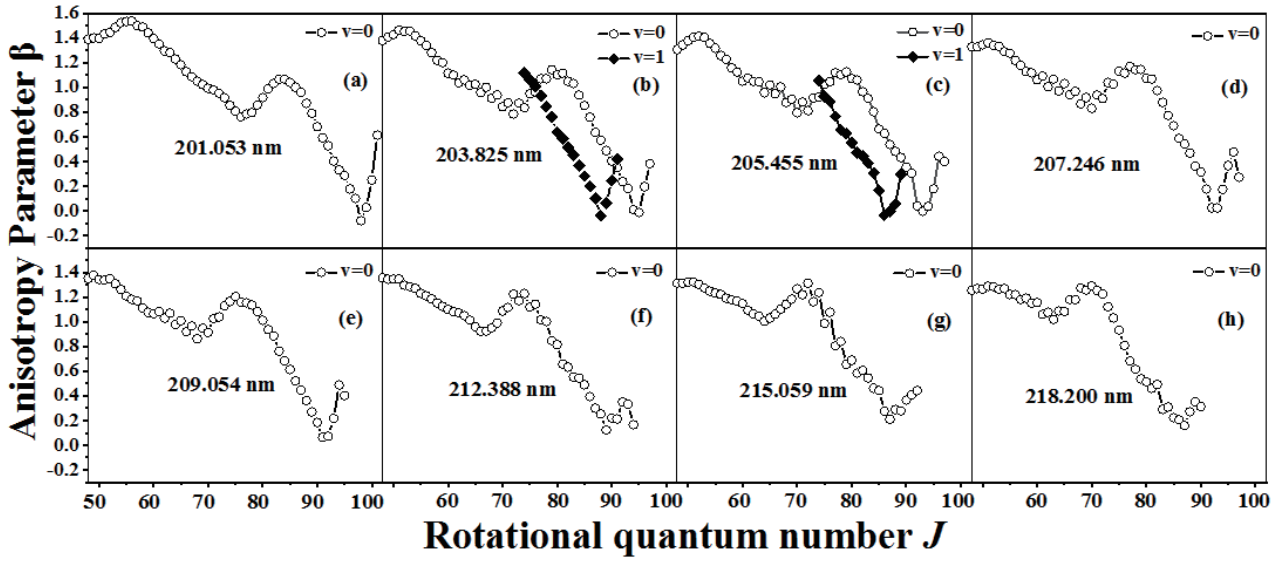

FIG. 5 The angular anisotropy β value as a function of rotational quantum number for N_2 photofragments at all photolysis wavelengths.

different contributions to N_2 products with different rotational quantum numbers. The higher rotational quantum number, the larger proportion of N_2 products is from $1^1A''$ state excitation. This is basically consistent with Neyer's perspective [41].

FIG. 5 shows the rotational state dependent anisotropy parameter β at eight photolysis wavelengths. It is clear that for $N_2(v=0)$ at 203.825 nm, β declines slowly with increasing J from $\beta \approx 1.4$ at the low end of the rotational distribution near $J=50$ to a value of 0.8 near $J=70$, then β increases a little around the maximum of the rotational distribution near $J \approx 80$. It then declines more steeply, reaching $\beta \approx 0$ at $J=95$, and increases again near the high end of the rotational distribution. The similar trends of β values as a function of J are observed at all studied wavelengths in this work and also for $N_2(v=1)$ products. The impulsive model was used by Neyer *et al.* [31] to interpret the variation of the β value of N_2 fragments with J. They suggested that the greater bending angle of the molecule relative to its linear configuration within excitation to the $2^1A'$ excited state produces the higher rotational excited state of the N_2 fragments and the less β value. This model only qualitatively elucidated the decreasing tendency of β valve with the increase of J to a certain extent, but it cannot fit the β-J curves well. Recent theoretical works by McBane *et al.* [23] quantitatively illustrated the change of β-J curves by using trajectory surface hopping (TSH) method, and reproduced both the slower decline for $J<80$ and the steeper decline at higher J. The first decrease in the β value when $J<65$ is dominantly owing to the change in the direction of the transition dipole moment from the $2^1A'$ state to the ground state. While the sharp decrease in β value after $J>80$ is attributed to the stronger torque in the "isomerization pathway" on the ground state potential energy surface (PES), resulting in the increase of non-axial recoil forces when the molecular bond is breaking. It can be simply understood that the O atom will be attracted by the terminal N atom following the bond angle of the molecule is $>90°$, and further stay away from the initial direction, causing the β value to decrease. Besides the two declines in the β values, FIG. 5 displays a little increase in the range $70<J<80$. As demonstrated by McBane *et al.* [23], the decrease in the observed β with J in the main part of the rotational distribution does not come from a change in the extent of nonaxial recoil. Instead, it arises because of the mutual dependence of J and transition dipole on the initial N_2 bond length. Theoretical predictions [23] gave nearly constant β value of 0.8 within the rotational distribution of $65 \le J \le 80$, which is qualitatively consistent with the experimental observation. FIG. 5 also displays a little increase of the β value at the end of high-J tail. We speculate that this may be because the repulsion between the O atom and the terminal N atom gradually takes over the dominant role of attraction after the bond angle is bent to a certain angle. If the excess energy ($h\nu$-D_0-TKER) is strong enough, it can overcome the repulsion and continue to bend at a certain angle.

DOI: 10.1063/1674-0068/cjcp2312135

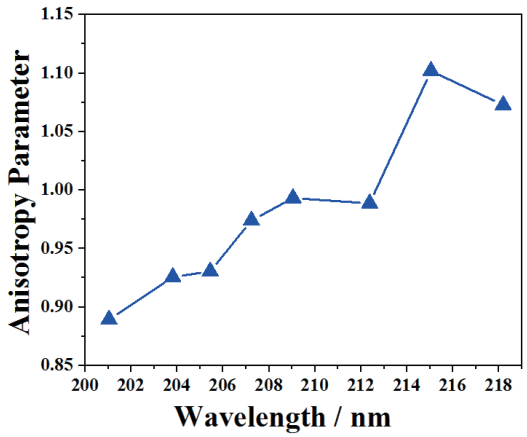

FIG. 6 The average β value as a function of the photolysis wavelength.

FIG. 6 shows the overall β value of the photofragments as a function of photolysis wavelengths. As the wavelength decreases, the β value decreases. This may be because different wavelengths will excite N_2O molecules to different Franck-Condon region, and different β value arises principally from nonaxial recoil due to the bending forces present in the excited state. The theoretical model [23] predicted the overall β value is about 0.9 at 203.25 nm, which is exactly consistent with our experimental observation. In one-color experiments, however, due to the influence arising from the detection process caused by alignment of O, it is hard to acquire the true angular anisotropy parameter.

IV. CONCLUSION

We have reinvestigated the photodissociation dynamics of $O(^1D)+N_2(X^1\Sigma_g^+)$ product channel from N_2O in the UV region by using time-sliced velocity-mapped ion imaging technique combined with single VUV photoionization scheme of $O(^1D)$ fragments at 99.95 nm. The TKER spectra of the products at eight photolysis wavelengths between 200 nm and 220 nm have been obtained, and the N_2 products are dominantly populated in $v=0$ with high rotational excitation. The anisotropy parameter β value as a function of rotational quantum number J for the N_2 product has been determined. Though the primary features are similar to that predicted by previous theoretical models, some discrepancies are still observed in both rotational state distributions and angular distributions. Further theoretical works are needed to clarify these discrepancies. This work provides the most detailed information in the state-to-state photodissociation dynamics of triatomic molecules.

V. ACKNOWLEDGEMENTS

The experimental work is supported by the National Natural Science Foundation of China (No.22241304, No.22225303), the National Natural Science Foundation of China (NSFC Center for Chemical Dynamics, No.22288201), the Scientific Instrument Developing Project of the Chinese Academy of Sciences (No.GJJSTD20220001), the Innovation Program for Quantum Science and Technology (No.2021ZD0303304). Xueming Yang also thanks the Guangdong Science and Technology Program (No.2019ZT08L455 and No.2019JC01X091), and the Shenzhen Science and Technology Program (No.ZDSYS20200421111001787).

[1] M. K. W. Ko, P. A. Newman, S. Reimann, and S. E. Strahan, *Lifetimes of Stratospheric Ozone-Depleting Substances, Their Replacements, and Related Species*, Zürich: SPARC Report No. 6, WCRP-15, (2013).

[2] M. J. Prather, J. Hsu, N. M. DeLuca, C. H. Jackman, L. D. Oman, A. R. Douglass, E. L. Fleming, S. E. Strahan, S. D. Steenrod, O. A. Sovde, I. S. Isaksen, L. Froidevaux, and B. Funke, J. Geophys. Res. Atmos. **120**, 5693 (2015).

[3] A. R. Ravishankara, A. L. Pele, L. Zhou, Y. Ren, A. Zogka, V. Daele, M. Idir, S. S. Brown, M. N. Romanias, and A. Mellouki, Phys. Chem. Chem. Phys. **21**, 24592 (2019).

[4] D. C. E. Bakker, H. W. Bange, N. Gruber, T. Johannessen, R. C. Upstill-Goddard, A. V. Borges, B. Delille, C. R. Löscher, S. W. A. Naqvi, A. M. Omar, and J. M. Santana-Casiano, *Air-Sea Interactions of Natural Long-Lived Greenhouse Gases (CO_2, N_2O, CH_4) in a Changing Climate*, Berlin, Heidelberg: Springer, (2014).

[5] K. Paustian, J. Lehmann, S. Ogle, D. Reay, G. P. Robertson, and P. Smith, Nature **532**, 49 (2016).

[6] H. Tian, R. Xu, J. G. Canadell, R. L. Thompson, W. Winiwarter, P. Suntharalingam, E. A. Davidson, P. Ciais, R. B. Jackson, G. Janssens-Maenhout, M. J. Prather, P. Regnier, N. Pan, S. Pan, G. P. Peters, H. Shi, F. N. Tubiello, S. Zaehle, F. Zhou, A. Arneth, G. Battaglia, S. Berthet, L. Bopp, A. F. Bouwman, E. T. Buitenhuis, J. Chang, M. P. Chipperfield, S. R. S. Dangal, E. Dlugokencky, J. W. Elkins, B. D. Eyre, B. Fu, B. Hall, A. Ito, F. Joos, P. B. Krummel, A. Landolfi, G. G. Laruelle, R. Lauerwald, W. Li, S. Lienert, T. Maavara, M. MacLeod, D. B. Millet, S. Olin, P. K. Patra, R. G. Prinn, P. A. Raymond, D. J. Ruiz, G. R.

van der Werf, N. Vuichard, J. Wang, R. F. Weiss, K. C. Wells, C. Wilson, J. Yang, and Y. Yao, Nature **586**, 248 (2020).
[7] K. Minschwaner, R. J. Salawitch, and M. B. McElroy, J. Geophys. Res. Atmos. **98**, 10543 (1993).
[8] D. J. Griggs and M. Noguer, Weather **57**, 267 (2002).
[9] M. Tsuji, M. Kawahara, K. Noda, M. Senda, H. Sako, N. Kamo, T. Kawahara, and K. S. Kamarudin, J. Hazard. Mater. **162**, 1025 (2009).
[10] T. Yamashita and A. Vannice, J. Catal. **161**, 254 (1996).
[11] X. D. Wang, X. F. Gao, C. J. Xuan, and S. X. Tian, Nat. Chem. **8**, 258 (2016).
[12] Z. Lu, Y. C. Chang, Q. Z. Yin, C. Y. Ng, and W. M. Jackson, Science **346**, 61 (2014).
[13] D. Rösch, Y. F. Xu, H. Guo, X. X. Hu, and D. L. Osborn, J. Phys. Chem. Lett. **14**, 3084 (2023).
[14] Y. Chang, Y. L. Fu, Z. C. Chen, Z. J. Luo, Y. R. Zhao, Z. X. Li, W. Q. Zhang, G. R. Wu, B. N. Fu, D. H. Zhang, M. N. R. Ashfold, X. M. Yang, and K. J. Yuan, Chem. Sci. **14**, 8255 (2023).
[15] Y. Chang, Y. Yu, F. An, Z. J. Luo, D. H. Quan, X. Zhang, X. X. Hu, Q. M. Li, J. Y. Yang, Z. C. Chen, L. Che, W. Q. Zhang, G. R. Wu, D. Q. Xie, M. N. R. Ashfold, K. J. Yuan, and X. M. Yang, Nat. Commun. **12**, 2476 (2021).
[16] K. Yoshino, D. E. Freeman, and W. H. Parkinson, Planet. Space Sci. **32**, 1219 (1984).
[17] S. Nanbu and M. S. Johnson, J. Phys. Chem. A **108**, 8905 (2004).
[18] R. Schinke, J. Chem. Phys. **134**, 064313 (2011).
[19] M. N. Daud, Int. J. Quantum Chem. **116**, 452 (2016).
[20] M. N. Daud, G. G. Balint-Kurti, and A. Brown, J. Chem. Phys. **122**, 54305 (2005).
[21] R. Schinke, J. Suarez, and S. C. Farantos, J. Chem. Phys. **133**, 091103 (2010).
[22] R. Schinke and J. A. Schmidt, J. Phys. Chem. A **116**, 11083 (2012).
[23] G. C. McBane and R. Schinke, J. Chem. Phys. **136**, 044314 (2012).
[24] G. Paraskevopoulos and R. Cvetanovic, J. Am. Chem. Soc. **91**, 7572 (1969).
[25] Y. F. Zhu and R. J. Gordon, J. Chem. Phys. **92**, 2897 (1990).
[26] R. Schinke, J. A. Schmidt, and M. S. Johnson, J. Chem. Phys. **135**, 194303 (2011).
[27] P. Felder, B. M. Haas, and J. Robert Huber, Chem. Phys. Lett. **186**, 177 (1991).
[28] L. L. Springsteen, S. Satyapal, Y. Matsumi, L. M. Dobeck, and P. L. Houston, J. Phys. Chem. **97**, 7239 (1993).
[29] T. F. Hanisco and A. C. Kummel, J. Phys. Chem. **97**, 7242 (1993).
[30] T. Suzuki, H. Katayanagi, Y. X. Mo, and K. Tonokura, Chem. Phys. Lett. **256**, 90 (1996).
[31] D. W. Neyer, A. J. R. Heck, and D. W. Chandler, J. Chem. Phys. **110**, 3411 (1999).
[32] T. Nishide and T. Suzuki, J. Phys. Chem. A **108**, 7863 (2004).
[33] Z. X. Li, M. Zhao, T. Xie, Y. Chang, Z. J. Luo, Z. C. Chen, X. A. Wang, K. J. Yuan, and X. M. Yang, Mol. Phys. **119**, e1813911 (2021).
[34] J. M. Zhou, Y. R. Zhao, C. S. Hansen, J. Y. Yang, Y. Chang, Y. Yu, G. K. Cheng, Z. C. Chen, Z. G. He, S. R. Yu, H. B. Ding, W. Q. Zhang, G. R. Wu, D. X. Dai, C. M. Western, M. N. R. Ashfold, K. J. Yuan, and X. M. Yang, Nat. Commun. **11**, 1547 (2020).
[35] Z. X. Li, M. Zhao, T. Xie, Z. J. Luo, Y. Chang, G. K. Cheng, J. Y. Yang, Z. C. Chen, W. Q. Zhang, G. R. Wu, X. A. Wang, K. J. Yuan, and X. M. Yang, J. Phys. Chem. Lett. **12**, 844 (2021).
[36] Y. R. Zhao, Z. J. Luo, Y. Chang, Y. C. Wu, S. E. Zhang, Z. X. Li, H. B. Ding, G. R. Wu, J. S. Campbell, C. S. Hansen, S. W. Crane, C. M. Western, M. N. R. Ashfold, K. J. Yuan, and X. M. Yang, Nat. Commun. **12**, 4459 (2021).
[37] M. Zhao, Z. X. Li, T. Xie, Y. Chang, F. Y. Wu, Q. Wang, W. T. Chen, T. Wang, X. A. Wang, K. J. Yuan, and X. M. Yang, Chin. J. Chem. Phys. **34**, 95 (2021).
[38] Y. Chang, M. N. R. Ashfold, K. J. Yuan, and X. M. Yang, Nat. Sci. Rev. **10**, nwad158 (2023).
[39] A. G. Smolin, O. S. Vasyutinskii, E. R. Wouters, and A. G. Suits, J. Chem. Phys. **121**, 6759 (2004).
[40] H. Kawamata, H. Kohguchi, T. Nishide, and T. Suzuki, J. Chem. Phys. **125**, 133312 (2006).
[41] D. W. Neyer, A. J. R. Heck, D. W. Chandler, J. M. Teule, and M. H. M. Janssen, J. Phys. Chem. A **103**, 10388 (1999).
[42] J. M. Teule, G. C. Groenenboom, D. W. Neyer, D. W. Chandler, and M. H. M. Janssen, Chem. Phys. Lett. **320**, 177 (2000).
[43] D. J. Harding, J. Neugebohren, M. Grutter, A. F. Schmidt-May, D. J. Auerbach, T. N. Kitsopoulos, and A. M. Wodtke, J. Chem. Phys. **141**, 054201 (2014).
[44] J. A. Schmidt, M. S. Johnson, U. Lorenz, G. C. McBane, and R. Schinke, J. Chem. Phys. **135**, 024311 (2011).
[45] S. M. Wu, D. Chestakov, G. C. Groenenboom, W. J. van der Zande, D. H. Parker, G. R. Wu, X. M. Yang, and C. Vallance, Mol. Phys. **108**, 1145 (2010).
[46] I. Wilkinson, M. P. de Miranda, and B. J. Whitaker, J. Chem. Phys. **131**, 054308 (2009).
[47] A. Kramida, Y. Ralchenko, J. Reader, and NIST ASD Team, *NIST Atomic Spectra Database (ver. 5.11)*, Gaithersburg: National Institute of Standards and Technology, (2023).
[48] A. Brown, P. Jimeno, and G. G. Balint-Kurti, J. Phys. Chem. A **103**, 11089 (1999).

DOI: 10.1063/1674-0068/cjcp2312135